AIAA JOURNAL
Vol. 34, No. 12, December 1996

Computational Study of the Flowfields Associated with Oblique Shock/Vortex Interactions

Ashish Nedungadi* and Mark J. Lewis†
University of Maryland, College Park, Maryland 20742-3015

The interaction between a supersonic streamwise vortex and an oblique shock is solved numerically using the unsteady, three-dimensional Euler equations. The parametric study ascertains the effects of vortex strength, streamwise velocity deficit, and Mach number on the oblique shock/vortex interaction. The vortex, whose tangential and streamwise velocities are analytically modeled, is introduced upstream of the shock and allowed to interact with the shock. The interaction is examined at freestream Mach numbers of 3 and 5, using vortices of varying strength and possessing various velocity deficits. Three distinct types of interactions—weak, moderate, and strong—are observed, depending very strongly on the streamwise velocity deficit and, to a lesser degree, on the strength of the vortex. The weak interaction is characterized by a slight distortion of the shock and vortex with the resulting flowfield being supersonic everywhere. The moderate interaction, however, results in a more pronounced distortion of the shock, creating a small pocket of subsonic flow downstream of the interaction. In addition, the incident vortex is highly distorted by the shock and eventually splits up into two counter-rotating vortices. In the strong interaction, due to the formation of a large subsonic region, a dramatic reorganization of the original shock occurs, accompanied by a region of reversed subsonic flow, a stagnation point, and a drastic expansion of the vortex core, all of which are characteristics of vortex breakdown.

Nomenclature

M = Mach number
p = pressure, N/m^2
r_c = vortex core radius, 0.003 m
S = vortex swirl parameter, $\Gamma_0/(V_{x,\text{axis}}\, r_c)$
V_x = axial or streamwise velocity, m/s
V_θ = tangential velocity, m/s
Γ_0 = vortex circulation, m^2/s
λ = vortex strength parameter, S/Φ^3
μ = vortex strength parameter, τ/Φ^3
ρ = density, kg/m^3
τ = swirl ratio, $V_{\theta,\max}/V_{x,\text{axis}}$
Φ = ratio of axial to freestream velocity, $V_{x,\text{axis}}/V_\infty$

Subscripts

axis = conditions at vortex center, $r = 0$
0 = stagnation conditions
1 = conditions upstream of bubble shock (see Fig. 1)
2 = conditions in recirculation region (see Fig. 1)
∞ = freestream conditions

Introduction

THE interaction between a supersonic streamwise vortex and a shock wave, commonly known as a shock/vortex interaction (SVI), is a fundamental fluid dynamics problem with numerous applications. For example, vortices shed by the forebody of a high-speed vehicle, flying at high angles of attack, may pass through shocks generated from wings or other control surfaces. If the interaction is strong enough, the resulting flowfield can severely affect the aerodynamic characteristics of the vehicle. Another undesirable situation is one in which a vortex interacts with the shock system of a supersonic inlet. This SVI can adversely affect engine performance[1] and result in an unstart of the engine. An area in which the SVI can be advantageous is fuel–air mixing in a supersonic combustion ramjet where the addition of swirl increases the surface area over which the fuel and air interact. The main thrust behind this technique is either to increase the vorticity after the interaction and/or to redistribute the available vorticity such that fuel and air can come into contact with each other, resulting in improved mixing and combustion.

The vortex breakdown phenomenon in low-speed flows has been studied extensively, and several comprehensive survey papers[2–5] have been presented. Vortex breakdown is a scenario in which a rapid expansion of the vortex core takes place together with the formation of a stagnation point at the vortex axis. In addition, a region of reversed flow exists downstream of the stagnation point. Vortex breakdown and SVI research in high-speed, compressible flows have attracted serious attention only recently. Two distinct types of SVI can be considered: normal shock/vortex interaction (NSVI) and oblique shock/vortex interaction (OSVI). Delery et al.[6] conducted an experimental study on NSVI in which they defined a vortex breakdown limit as a function of vortex swirl ratio and shock intensity for Mach numbers between 1.6 and 2.28. Delery et al.[6] also performed Euler calculations of the interaction, which provided good agreement with the experimental breakdown limit. Vortex breakdown, characterized by a closed reverse flow bubble on the vortex axis, was also reported. Experimental work in NSVI by several researchers[7–10] has shown that vortex breakdown and an attendant flow unsteadiness is common in such interactions. All of these researchers observed that NSVI is more likely to result in vortex breakdown than OSVI because of the large pressure gradient imposed by the normal shock and the fact that the flow behind the shock was subsonic, allowing disturbances to propagate upstream. The interaction of a streamwise vortex with an oblique shock has also been examined experimentally and various aspects of this flowfield have been presented. Kalkhoran[11] conducted experimental studies of OSVI at Mach 3 and found that the interaction resulted in a very complicated, three-dimensional, and unsteady flowfield. A later study by Smart and Kalkhoran[12] on OSVI concluded that, under certain conditions of the vortex and shock strength, the incident vortex could breakdown and result in the formation of a steady, separated shock structure.

On the numerical side, three-dimensional Euler solutions[13] of the interaction between a supersonic streamwise vortex and an oblique shock wave at Mach numbers of 2.28 and 5.0 were obtained. In this work neither vortex breakdown nor an appreciable change in vortex strength were observed; however, regions of reversed flow and a convex-concave shock shape were observed. Rizzetta[14] presented

Presented as Paper 95-2770 at the AIAA/ASME/SAE/ASEE Joint Propulsion Conference, San Diego, CA, July 10–12, 1995; received Sept. 26, 1995; revision received Aug. 20, 1996; accepted for publication Aug. 23, 1996; also published in *AIAA Journal on Disc*, Volume 2, Number 1.

*Graduate Research Assistant, Department of Aerospace Engineering. Student Member AIAA.

†Associate Professor, Department of Aerospace Engineering. Associate Fellow AIAA.

Table 1 Test matrix

Run no.	M_∞	Γ_0	Φ
(1 2 3)	3.0	0.4	(1.0 0.8 0.6)
(4 5 6)	3.0	0.8	(1.0 0.8 0.6)
(7 8 9)	5.0	0.4	(1.0 0.8 0.6)
(10 11 12)	5.0	0.8	(1.0 0.8 0.6)

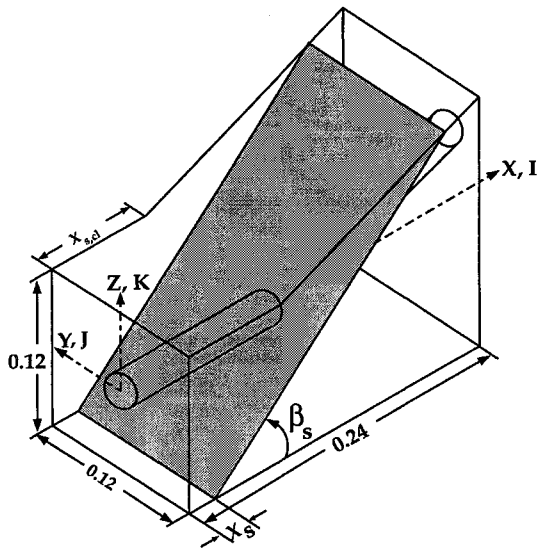

Fig. 1 Flowfield schematic of OSVI showing physical and computational coordinate systems.

Euler and Navier–Stokes simulations of OSVI, which were compared with experimental results. Overall, excellent agreement with experimental results was reported; however, vortex breakdown was not observed in this numerical simulation either. Rizzetta attributed this deficiency in the numerical calculations to the fact that the numerically generated vortex, due to a lack of quantitative experimental data, could not duplicate the conditions of the vortex in the experimental test.

Experimental[11,12] and numerical[14,15] work indicates that the streamwise velocity deficit within the vortex plays a pivotal role in causing vortex breakdown during an OSVI. Traditionally, the swirl ratio, $\tau' = V_{\theta,\max}/V_\infty$, and the swirl parameter, $S' = \Gamma_0/(V_\infty\, r_c)$, have been used to characterize the vortex strength. Cattafesta and Settles[8] point out that, because of the axial velocity deficit in the vortex, freestream velocity is not appropriate, and as such, a local value of velocity should be used. In this study, modified versions of these parameters are used, namely, $\tau = V_{\theta,\max}/V_{x,\text{axis}}$ and $S = \Gamma_0/(V_{x,\text{axis}}\, r_c)$. It is clear then that a vortex with a velocity deficit will tend to be stronger than vortices with a uniform streamwise velocity. This makes them more fragile and susceptible to vortex breakdown. The current work is designed to study the OSVI by employing a Burger's vortex model coupled with a streamwise velocity profile in which the vortex strength and the magnitude of the velocity deficit are varied. In addition, the OSVI is simulated at freestream Mach numbers of 3 and 5 at a freestream pressure and density of 1171.84 N/m^2 and 0.01476 kg/m^3, respectively. Figure 1 shows a schematic of the problem setup along with the physical and computational coordinate systems and dimensions, and Table 1 presents the Mach number, Γ_0, and Φ for each of the cases.

Numerical Formulation

The three-dimensional, unsteady, compressible Euler equations are used as the governing equations to simulate the interaction of a streamwise vortex with an oblique shock. For the flowfields that result in vortex breakdown, it is expected that viscous effects are small and might be important only in predicting the details of the flowfield structures. However, the inviscid equations can be used with confidence to predict the overall features and characteristics of the flowfield.

The numerical solutions are obtained using the general aerodynamic simulation program[16] (GASP 2.2), which solves the integral form of the time-dependent, Reynolds-averaged Navier–Stokes equations and its subsets. The code utilizes cell-centered, finite volume, characteristic-based (upwind) methods for the spatial discretization. The three-dimensional, unsteady Euler equations in integral form can be expressed as

$$\frac{\partial}{\partial t}\iiint_{\mathcal{V}} \boldsymbol{Q}\,\mathrm{d}\mathcal{V} + \iint_{S} \boldsymbol{F}\cdot\boldsymbol{n}\,\mathrm{d}S = 0 \tag{1}$$

where $\boldsymbol{Q} = [\rho\ \rho u\ \rho v\ \rho w\ \rho e_0]^T$ and $\boldsymbol{F}\cdot\boldsymbol{n} = \boldsymbol{F}\cdot\boldsymbol{i}+\boldsymbol{G}\cdot\boldsymbol{j}+\boldsymbol{H}\cdot\boldsymbol{k}$. The terms $\boldsymbol{F}$, $\boldsymbol{G}$, and $\boldsymbol{H}$ are the inviscid flux vectors in the i, j, and k directions, respectively. Equation (1) is reformulated in terms of the volume-averaged values of the conserved variables, $\langle\boldsymbol{Q}\rangle$, and the primitive variables, $\boldsymbol{q} = [\rho\ u\ v\ w\ p]^T$, as

$$\mathcal{V}\frac{\partial\langle\boldsymbol{Q}\rangle}{\partial\boldsymbol{q}}\frac{\partial\boldsymbol{q}}{\partial t} + \sum_{j=1}^{6}\boldsymbol{F}\cdot\boldsymbol{n}\,\mathrm{d}S = 0 \tag{2}$$

Equation (2) is solved numerically using an implicit three-factor approximate factorization approach, which results in a sequence of three block tridiagonal systems of equations. The first-order accurate Euler-implicit method is used for the time discretization. The cell-centered values of the inviscid flux vectors are calculated using Roe's flux difference-splitting[17] algorithm. To obtain the values of the fluxes at the cell faces, the cell-centered values are extrapolated using the monotone upstream-centered scheme for conservation laws (MUSCL). With this extrapolation scheme, a value for κ determines the spatial accuracy of the solution, and for the present analysis $\kappa = \frac{1}{3}$, resulting in a third-order upwind-biased algorithm. Though this unlimited extrapolation works well in the smooth regions of the flow, the higher-order corrections must be limited, in regions with large gradients, to maintain stability and eliminate spurious numerical oscillations. To this end, Roe's SuperBee limiter[18] is used in this work because it provides the least amount of numerical oscillations near the shocks and minimizes the diffusion of the vortex as it convects downstream.

Computational Grid

A three-dimensional algebraic grid is used in which the grid is clustered[19] about the centerline to accurately represent the circular vortex on a Cartesian mesh. Furthermore, grid clustering is essential to minimize the diffusion of the vortex as it convects downstream. Since the vortex deflects upward upon interacting with the oblique shock, as shown schematically in Fig. 1, the upper boundary of the computational domain is turned upward after the point where the shock intersects the centerline ($X_{s,\text{cl}}$). The Z coordinate of the upper boundary is expressed as

$$Z = \begin{cases} L_z/2 & X \le X_{s,\text{cl}} \\ (X - X_{s,\text{cl}})\tan\theta_s + (L_z/2) & X \ge X_{s,\text{cl}} \end{cases} \tag{3}$$

where $L_z = 0.12$ m is the domain height at the inflow plane and $\theta_s = 23.3$ deg is the flow deflection angle.

To study the effects of grid resolution, medium and fine meshes are also generated. The mesh sizes and their corresponding minimum and maximum grid spacings are presented in Table 2. In the medium and fine meshes, regions of grid clustering and the extent of the boundaries are identical to that of the coarse grid.

Boundary Conditions

The first step in obtaining a solution for an OSVI is to establish an oblique shock for a given freestream Mach number and flow turning angle. This is accomplished by introducing freestream conditions at

Table 2 Size and minimum grid spacing for the computational grids

Designation	Size	ΔX, mm	$\Delta Y = \Delta Z$, mm
Coarse	76 × 76 × 101	2.4	1.25
Medium	113 × 113 × 151	1.6	0.83
Fine	149 × 149 × 201	1.2	0.63

the inlet ($X = 0$) of the domain, as shown in Fig. 1. Instead of solving the flowfield over a wedge of semiangle, θ_s, the oblique shock is obtained by applying freestream and postshock conditions before and after $X = X_s$, respectively, on the lower boundary ($Z = -0.06$ m). This technique is particularly advantageous because it allows more grid points within the domain of interest. Second-order extrapolation is applied at the exit plane ($X = 0.24$ m), whereas first-order extrapolation is enforced at the two side boundaries ($Y = \pm 0.06$ m) and the upper boundary.

Once the oblique shock is generated, a streamwise vortex is introduced at $X = 0$ and is allowed to interact with the shock. The vortex is introduced by replacing the freestream conditions at the inlet plane with the vortex properties, which include p, ρ, and u, v, and w components of velocity. The tangential velocity is supplied by an analytical model[5] of a Burger's type vortex and is expressed as

$$V_\theta(r) = (\Gamma_0/r)\{1 - \exp[-(r/r_c)^2]\} \tag{4}$$

For this study, $r_c = 0.003$ m and is the vortex core radius. The v and w components of velocity are calculated from V_θ by transforming the preceding cylindrical coordinates (r, θ) to Cartesian coordinates (y, z). Experiments with vortices generated by flow over wing tips[12] and swirl vanes[8] have observed a deficit in the streamwise velocity V_x across the vortex. Cattafesta and Settles[8] have also observed a total temperature deficit, which ranges from 0.95 to 1.05 (of the freestream total temperature) at the vortex core to the outer edge, respectively. The deficit in velocity and total temperature has been postulated to be a result of the low energy in the boundary layer at the surfaces of the wing or swirl vanes. The effect of a total temperature variation will most probably manifest itself by altering the Mach number distribution through the vortex, but it is believed that this effect will be small and will not significantly affect the OSVI. Hence, for the present analysis, a constant total temperature is assumed. The axial velocity deficit is modeled using the following function[5]:

$$V_x(r) = V_\infty + V_\infty(\Phi - 1)\exp[-(r/b)^2] \tag{5}$$

where $b = 0.006$ m and is defined as a characteristic thickness of the profile.

The pressure distribution through the vortex is calculated by solving the radial momentum equation, $dp/dr = \rho V_\theta^2/r$. Making use of the equation of state and total enthalpy $H_0 = H_{0,\infty} = \text{const}$, ρ is expressed in terms of p, $H_{0,\infty}$, V_x, V_θ, and the ratio of specific heats γ. The radial momentum equation then becomes

$$\frac{dp}{dr} = \frac{\gamma}{\gamma - 1}\frac{p}{H_{0,\infty} - \frac{1}{2}(V_x^2 + V_\theta^2)}\frac{V_\theta^2}{r} \tag{6}$$

which is solved using a fourth-order Runge–Kutta scheme.

Results

Vortex Propagation

As the streamwise vortex convects downstream of the inflow plane, the vortex tends to diffuse, or become weaker, due to the inherent numerical dissipation present in the algorithm. The weakening of a vortex is characterized by an increase in the density (or pressure) at the vortex center ($r = 0$), a decrease in the magnitude of the peak tangential velocity, and an increase in the core radius. The changes in vortex properties are dependent on the grid resolution in the cross flow (Y–Z) plane and to a lesser extent on the streamwise resolution. In numerical[14] and experimental[12] work, it has been shown that the OSVI is highly dependent on the vortex strength, and as such, if the vortex diffuses to a large degree, the resulting interaction will be markedly different.

The vortex is convected without the oblique shock to verify that it is stable and that its properties do not change appreciably. For these calculations, the coarse grid is used in which the upper and lower boundaries are parallel. Figure 2 presents the normalized density and tangential velocity profiles through the centerline of the vortex, for run 11, at the inflow plane ($X = 0$), the location where the shock intersects the centerline ($X = 0.1$ m), and the exit plane ($X = 0.24$ m). The relative change in ρ_{axis} between $X = 0$ and 0.24 m is 6%. A more meaningful comparison is the change in ρ_{axis} between $X = 0$ and 0.1 m, which is only 0.08%. The V_θ distribution

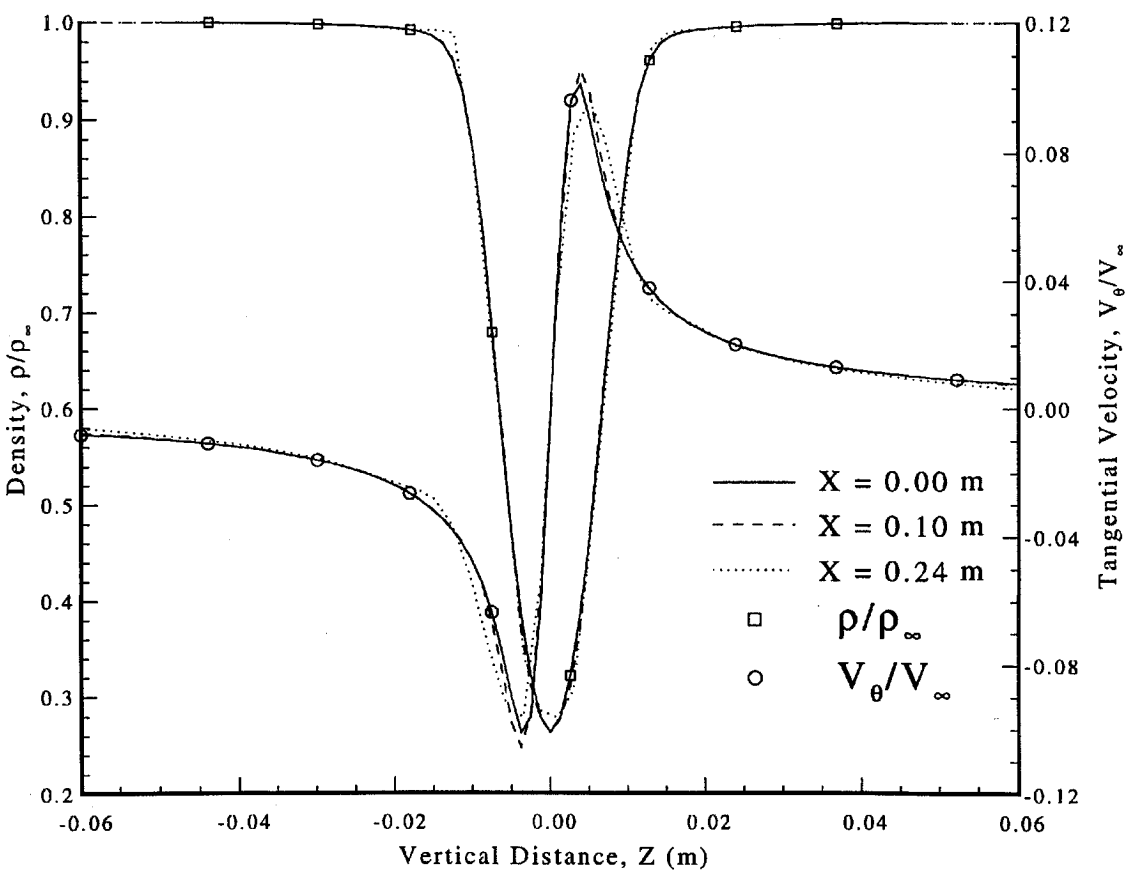

Fig. 2 Nondimensional density and tangential velocity profiles at various axial locations.

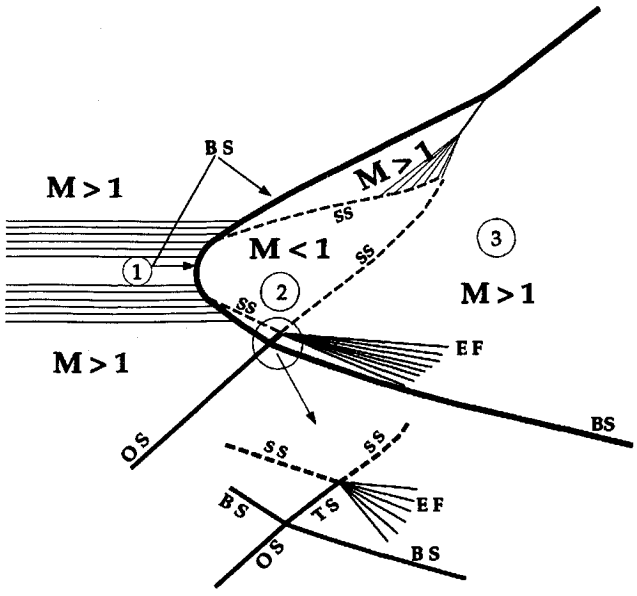

Fig. 3 Schematic of a strong OSVI. BS = bubble shock, OS = oblique shock, EF = expansion fan, SS = slip surface, and TS = transmitted shock.

shows that $|V_{\theta,\max}|$ and r_c change by 4.63 and 8%, respectively, between $X = 0$ and 0.24 m, whereas the change in the $|V_{\theta,\max}|$ between $X = 0$ and 0.1 m is negligible. It was observed that without grid clustering near the vortex, ρ_{axis} and r_c changed by as much as 30 and 20%, respectively.

Grid Resolution Study

The flowfield associated with run 3 is selected to perform a grid resolution study because it represents a strong OSVI (to be discussed later), which takes on a very complicated three-dimensional flowfield. To this end, run 3 is simulated on the coarse, medium, and fine grids, and the results are presented in terms of density contours as well as pressure distributions along various Z locations in the $Y = 0$ plane.

Before embarking on the discussion of the results, it is important to point out the salient features of this complex flowfield. Figure 3 presents a schematic of a typical strong OSVI. Region 2 consists of subsonic recirculating flow that the outer supersonic flow responds to as if it were a solid body. Consequently, a three-dimensional conical shock is formed upstream of the recirculation bubble. This shock is known as the bubble shock[7] and is normal at the vortex axis. In region 2, slip surfaces separate the subsonic and supersonic flows. A complicated shock–shock interaction takes place when the original oblique shock intersects the lower portion of the bubble shock, resulting in a transmitted shock, which in turn interacts with the slip surface to form an expansion fan. A more detailed discussion of these structures will be presented in a later section.

Figure 4 shows a plot of normalized density contours in the $Y = 0$ plane for the coarse, medium, and fine grids. The results between the three grids are similar and predict the same flowfield features. The coarse grid is found to be sufficiently fine to capture the essential features of the flowfield with the notable exception that the normal portion of the bubble shock is smeared out. The structure of the bubble shock can be clearly seen on the medium and fine grids.

Figure 5 shows normalized pressure distributions along $Z = -0.02$, 0.00, 0.02, and 0.05 m in the $Y = 0$ plane. Note that these constant Z lines are chosen to compare data for all three grids at the same location and as such do not correspond to streamlines of the flowfield. At $Z = -0.02$ m, there are two distinct pressure rises. The first is across the original oblique shock, and the second is across the continued bubble shock. The pressure decreases as it traverses the expansion fan and levels off at a value slightly below the pressure that would have existed behind the oblique shock. The distribution along $Z = 0$ shows a contant pressure within the vortex core, a

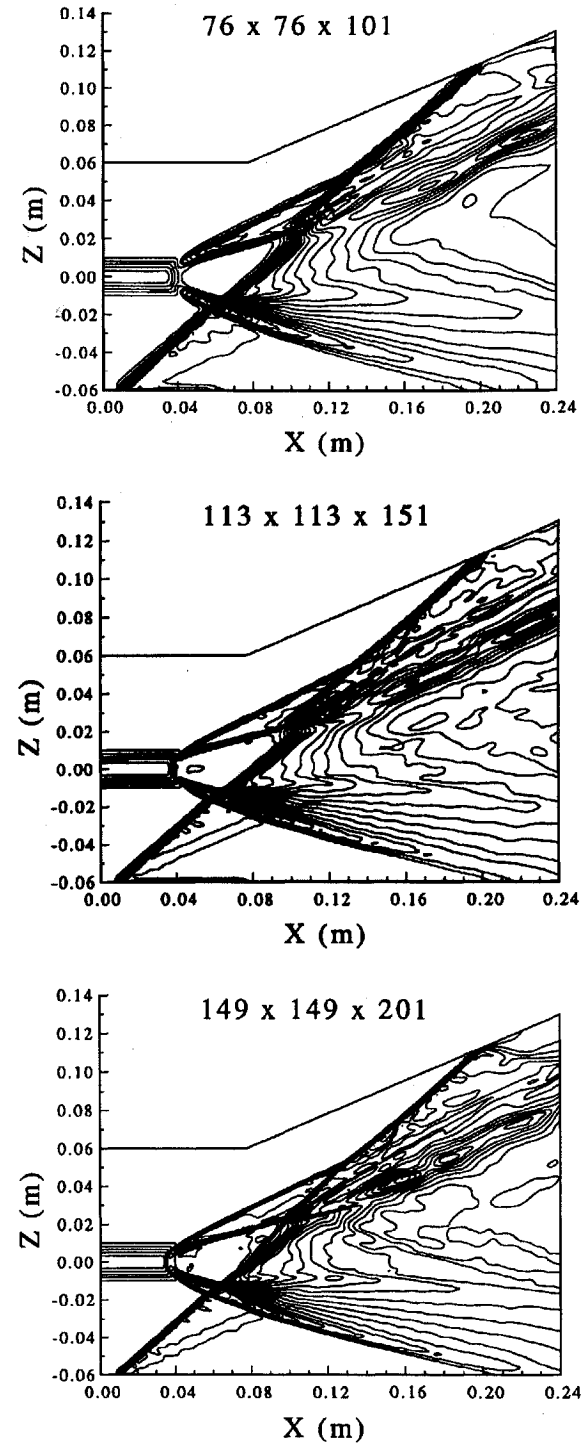

Fig. 4 Normalized density contours on $Y = 0$ plane for three different grid sizes.

sharp increase across the normal portion of the bubble shock, and a constant pressure region within the recirculation bubble. The local Mach number and p_1/p_∞, upstream of the bubble shock, at $Z = 0$ are 1.24 and 0.913, respectively. At these conditions, the theoretical stagnation pressure across a normal shock, $p_{0,2}/p_\infty = (p_{0,2}/p_{0,1})(p_{0,1}/p_1)(p_1/p_\infty) = (0.988)(2.556)(0.913) = 2.31$. The average pressure in the recirculation region predicted by all three grids is approximately 2.26, which is in excellent agreement to the theoretical stagnation pressure. Downstream of the recirculation region, the pressure increases and approaches the pressure that would have existed behind the oblique shock. The pressure variations along $Z = 0.02$ and 0.05 m are also shown in Fig. 5, confirming that the coarse grid captures the essential features of the flowfield and is deemed sufficiently fine for the purposes of this investigation.

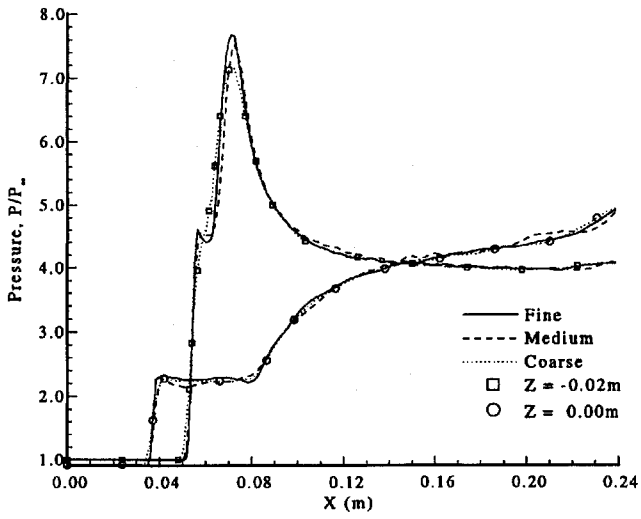

a) Z = −0.02 and 0.00 m

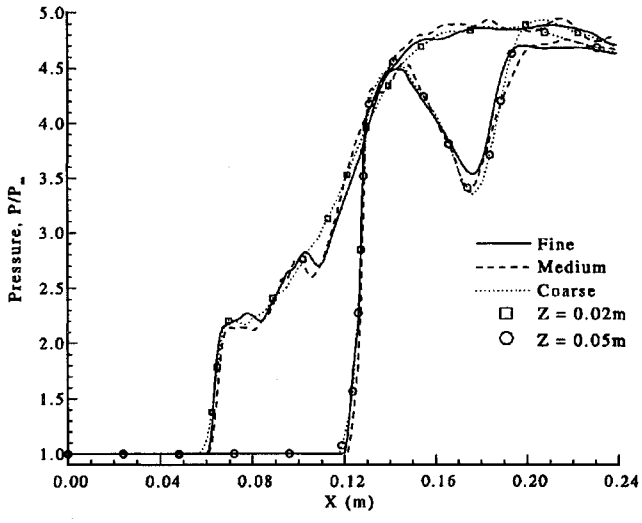

b) Z = 0.02 and 0.05 m

Fig. 5 Effect of grid resolution on streamwise pressure at various Z locations.

OSVI

The OSVI has been investigated at freestream Mach numbers of 3 and 5, using vortices of various strengths and streamwise velocity deficits. The velocity deficit is chosen such that the Mach number distribution through the vortex is supersonic and the vortex strengths are chosen for different values of Γ_0, which were chosen to match the experimental work of Cattafesta.[20]

Three different types of interactions are observed: weak, moderate, and strong. Each type of interaction is characterized by unique flowfield structures, and the features of each will be discussed separately. Two vortex strength parameters, namely, $\lambda \equiv S/\Phi^3$ and $\mu \equiv \tau/\Phi^3$, are introduced that, for the present parametric study, are able to classify each of the cases according to its interaction type. Table 3 presents a classification of each of the interactions in terms of λ and μ. For reference, the values of S and τ are also included.

Weak Interaction

In this work, weak interactions are characterized by a slight distortion of the shock and minimal change in the vortex structure. With the exception of run 8 for which $\Phi = 0.8$, all cases for which $\Phi = 1$ resulted in a weak interaction. In the region where the vortex intersects the shock, the shock distorts and takes on the convex-concave shape observed in previous numerical work.[13,14] The shock distortion is attributed to the fact that the vortex strikes the shock at different angles due to the nonuniform velocity distribution present in the vortex. Because of the formation of this curved shock, and depending on the level of shock distortion, weak expansion waves

Table 3 Classification of OSVI in terms of vortex strength parameters

Run no.	S	τ	λ	μ	Interaction type
7	0.078	0.050	0.078	0.050	Weak
1	0.131	0.083	0.131	0.083	Weak
10	0.157	0.100	0.157	0.100	Weak
8	0.098	0.063	0.191	0.122	Weak
4	0.261	0.167	0.261	0.167	Weak
2	0.163	0.104	0.319	0.203	Moderate
11	0.196	0.125	0.382	0.244	Moderate
9	0.131	0.083	0.607	0.386	Strong
5	0.327	0.208	0.639	0.407	Strong
3	0.218	0.139	1.010	0.643	Strong
12	0.261	0.167	1.208	0.772	Strong
6	0.435	0.278	2.013	1.286	Strong

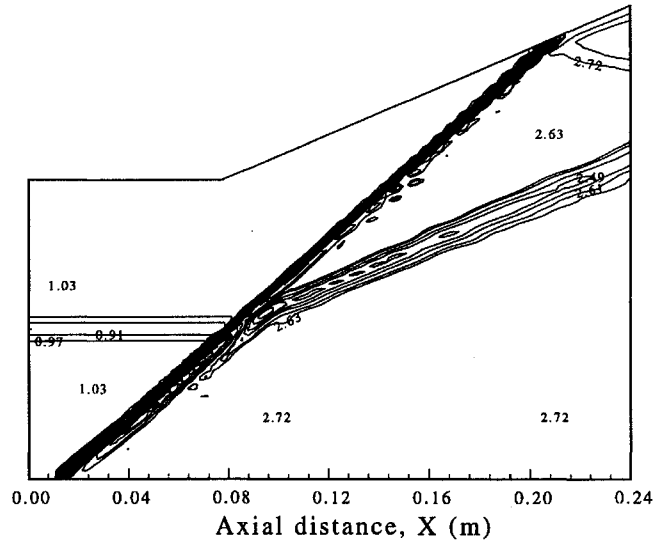

Fig. 6 Normalized density contours in the X–Z plane at Y = 0 for run 1.

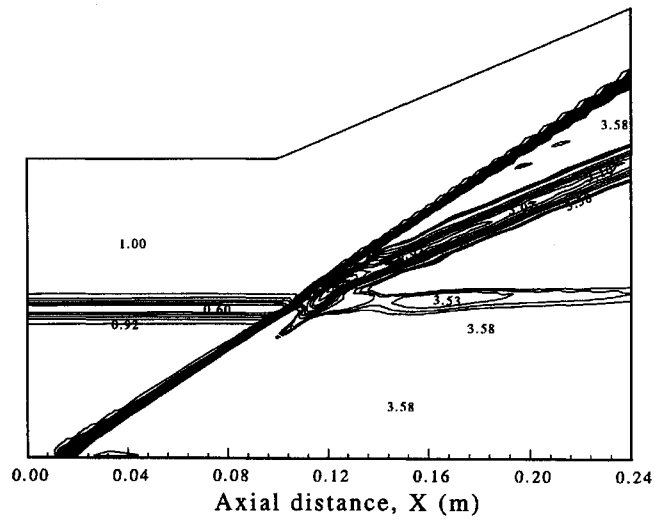

Fig. 7 Normalized density contours in the X–Z plane at Y = 0 for run 10.

emanate near the interaction region and travel toward the lower boundary. In fact, Smart and Kalkhoran[12] observed a decrease in pressure at their shock-generating surface and postulated that that was a consequence of expansion waves originating near the region of the interaction. The formation of these expansion waves is only observed in runs 4, 8, and 10 in which there was relatively more shock distortion compared with runs 1 and 7. The higher values of λ and μ for runs 4, 8, and 10 correctly predict that they result in relatively stronger interactions compared with runs 1 and 7.

Typical weak interaction flowfields are depicted in Figs. 6 and 7, which show the normalized density contours in the $Y = 0$ plane

for runs 1 and 10, respectively. The plots indicate that the incident vortex, upon striking the shock, deflects upward and convects downstream. The angle of deflection of the vortex for the weak interaction cases varied from 23.4–23.7 deg, which is approximately equal to the flow turning angle of $\theta_s = 23.3$ deg.

Figure 8 shows the normalized density contours in the Y–Z plane at $X = 0.144$ m. This figure describes the vortex structure after interacting with the oblique shock. As the vortex passes through the shock, it is compressed and acquires an elliptical shape with its major axis aligned with the Z axis. Furthermore, the vortex, in addition to being deflected upward, is deflected to the left looking downstream of the inflow plane.

Moderate Interaction

The term moderate interaction is used to refer to one in which the incident vortex does not breakdown; however, the properties of the vortex are such that it distorts the shock wave to such a degree as to produce a subsonic region immediately behind the shock. Figure 9 shows a nondirectional, computationally generated schlieren type plot ($|\nabla\rho|$) for run 2, which, along with run 11, results in such a flowfield. Although the Mach 5 case (run 11) has a larger Γ_0 and interacts with a stronger shock than the Mach 3 case (run 2), it results in a moderate interaction. The reason for this could be the fact that the Mach 5 flow has a higher axial velocity at the vortex center ($V_{x,\text{axis}} = 1361$ m/s) than the Mach 3 vortex ($V_{x,\text{axis}} = 812$ m/s) and hence possesses higher kinetic energy to be able to withstand the work associated with the higher pressure gradient. The analogy of boundary-layer separation under an adverse pressure gradient can be drawn for this scenario; if the flow along the surface has sufficient kinetic energy, it is able to withstand the adverse pressure gradient and remain attached.

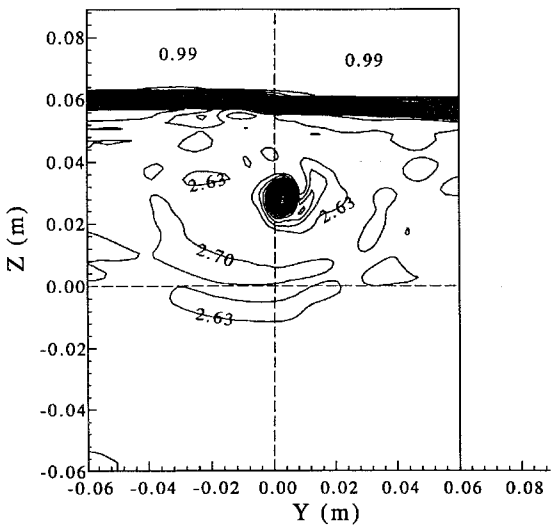

Fig. 8 Normalized density contours in the Y–Z plane at $X = 0.144$ for run 4.

As the vortex passes through the shock, it distorts the oblique shock to such a degree as to form a nearly normal shock at the centerline as can be seen in the magnified view of Fig. 9. For run 2, $M_{1,\text{axis}} = 1.87$ and $M_{2,\text{axis}} = 0.82$. The term $M_{2,\text{axis}}$ is higher than the Mach number for a normal shock, indicating that the distorted shock is not normal but is rather a strong oblique shock that produces a small region of subsonic flow behind it. Another possible explanation for the formation of a nearly normal shock at the centerline is that the centerline Mach number is less than that required for an attached shock for $\theta_s = 23.3$ deg. The increased distortion of the shock as compared with the weak interaction is largely attributed to the deficit in Mach number through the vortex core. It does not appear as though the vortex strength plays a very strong role in determining the type of interaction because it is observed that run 4, which has a stronger vortex than run 2, results in a weak interaction. The difference between these two cases is that run 2 has a Mach number deficit whereas run 4 does not. The higher values of λ and μ of run 2 predict that it will result in a stronger interaction than run 4.

Just as the vortex distorts the oblique shock, there is also a distortion of the vortex due to the shock. In the weak interaction, the vortex distortion is minimal; however, for the moderate interaction, the shock compresses the vortex to a larger extent and the incident vortex splits into two counter-rotating vortices. In experimental work on OSVI, Cattafesta and Settles[8] also observed this phenomenon of the incident vortex splitting up into two elliptically shaped vortices downstream of the interaction. The center of the primary vortex is deflected to the left ($Y = 0.0082$ m), whereas the secondary vortex center is deflected to the right ($Y = -0.0082$ m) as illustrated by the density contour plot of Fig. 10. The splitting up of the vortex is also observed for run 2.

Strong Interaction

The term strong interaction is used here to refer to one that results in vortex breakdown. To the best of the authors' knowledge, vortex

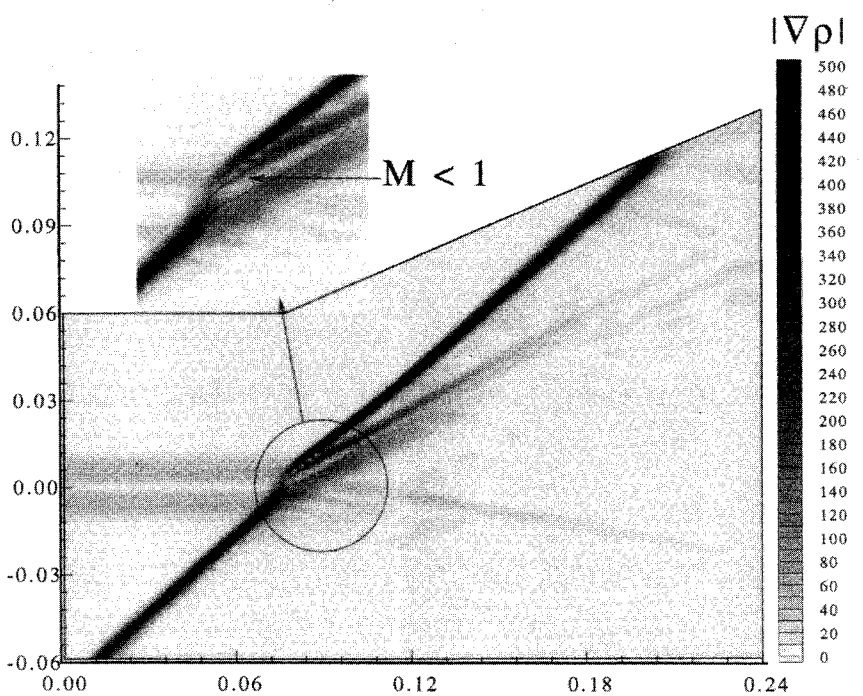

Fig. 9 Computational schlieren for run 2 and depiction of subsonic region. Units of $\nabla\rho$ are 1/m.

breakdown has not been previously simulated numerically for an OSVI. Although experimental work[12] has alluded to the possible existence of vortex breakdown, previous numerical simulations[13,14] have been unable to predict vortex breakdown. Earlier numerical work[13] suggested that vortex breakdown may not occur for OSVI because the flowfield behind the shock remains supersonic, but that appears not to be the case in the present calculations. Vortex breakdown is observed for runs 3, 5, 6, 9, and 12, but for the purpose of discussion, only the results of runs 3 and 12 are presented. To assist with the description of this complicated three-dimensional flowfield, a schematic of a strong interaction has been presented in Fig. 3.

Figure 11 shows a contour plot of $|\nabla\rho|$, whereas Fig. 12 presents a detailed view of the recirculation bubble in the $Y = 0$ plane for run 3. The incident vortex interacts with the oblique shock and, because of the relatively low Mach number within the vortex core, creates a subsonic region downstream of the shock. In fact, it is observed that the initial formation of the subsonic region begins slightly below the vortex axis. It is speculated that because the relatively low Mach number within the vortex cannot be sustained by the high pressure gradient of the oblique shock, the only possible solution is a detached shock with subsonic flow behind it. The moderate interactions also result in a small subsonic region; however, it is small and does not grow with time. It is believed that since the subsonic region in the moderate interaction is caused by a strong oblique shock, no information is propagated upstream. The subsonic region in the strong interaction, on the other hand, resulting from a detached shock, does allow upstream information propagation.

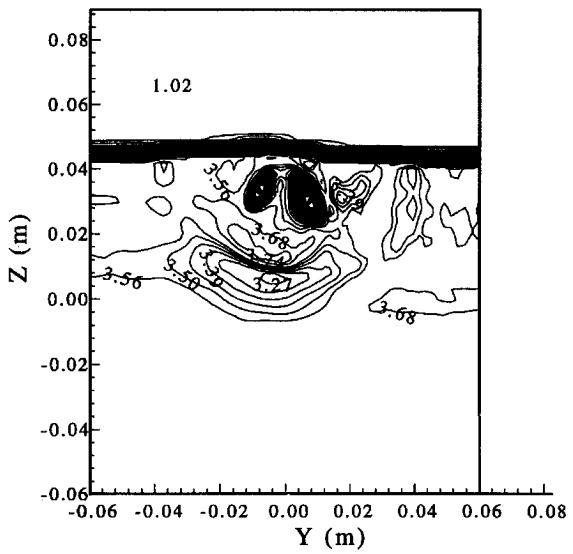

Fig. 10 Normalized density contours in Y–Z plane at $X = 0.168$ for run 11.

This subsonic region, labeled as region 2 in Fig. 3, grows with time and contains recirculating flow, as illustrated in Fig. 12. This region, referred to as the recirculation bubble, in essence acts as a solid conical body in a supersonic stream. The outer supersonic flow then responds to this apparent solid body by creating a locally three-dimensional conical shock upstream of the recirculation bubble. This curved shock is called a bubble shock and is normal to the vortex axis. The velocity at the axis, V_x/V_∞, decreases to 0.03 downstream of the bubble shock. This seems to indicate that in region 2, downstream of the bubble shock, a stagnation point does indeed occur at the vortex axis. In a previous section it was shown that the static pressure across the normal portion of the bubble shock (see Fig. 5 for $Z = 0$) corresponds very closely to the stagnation pressure across a normal shock. These two results strongly indicate the possibility of a stagnation point at the vortex axis, which is universally considered to be a characteristic of vortex breakdown. In their experimental work, Smart and Kalkhoran[12] also observed this separated shock structure for a strong vortex interacting with a strong oblique shock. Although the existense of a reversed flow region and stagnation point was alluded to, these features could not be measured directly. In the present study, each case resulting in a strong interaction is accompanied by a region of reversed flow. It should be pointed out that, although the main features of this strong interaction agree very well with experimental results, the exact features of vortex breakdown cannot be determined without ascertaining the effects of viscosity and turbulence, which have been excluded from this study.

In region 2 a slip surface above and below the axis separates the subsonic recirculating flow from the supersonic region. The reason for this is because the flow processed by the strongest part of the bubble shock is subsonic, whereas that processed by the weaker portion remains supersonic. Since the flow in region 3 is supersonic, an additional slip surface is required to separate this region from region 2. These three slip surfaces are clearly indicated in

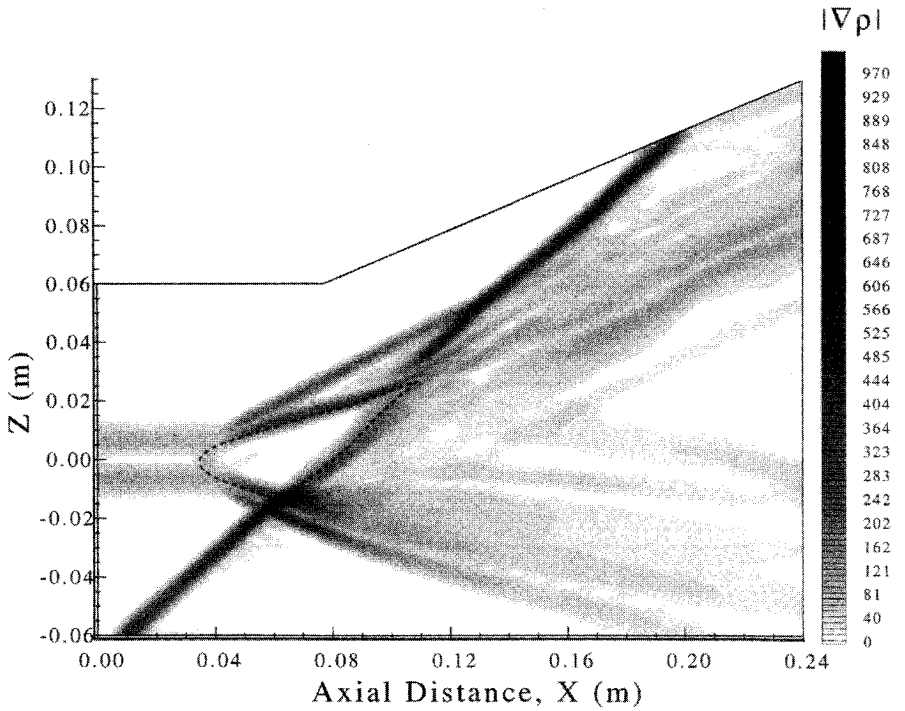

Fig. 11 Computational schlieren in $Y = 0$ plane for run 3 with a superimposed Mach 1 contour. Units of $\nabla\rho$ are 1/m.

the schlieren plot in Fig. 11. A transmitted shock is created by the interaction of the original oblique shock and the lower portion of the bubble shock. The transmitted shock terminates at and interacts with the slip surface, giving rise to an expansion fan. This region is one of very high pressure and temperature as indicated by the pressure distribution along $Z = -0.02$ m in Fig. 5. The bubble shock continues through the oblique shock and begins to curve slightly as the expansion waves strike the shock surface. The continuation of the bubble shock through the undisturbed oblique shock has been observed in previous experimental[12] work on OSVI. The continued bubble shock weakens as it propagates downstream, and this could be attributed to a combination of a three-dimensional relieving effect as well as the interaction of the expansion waves. The upper portion of the bubble shock induces a nonuniform flowfield, resulting in an upstream displacement of the original oblique shock, and the shock structures merge to form a single shock.

Figure 13 shows a contour plot of $|\nabla\rho|$ in the $Y = 0$ plane for run 12, which illustrates the features of the vortex breakdown for the Mach 5 case. Qualitatively, this flowfield is very similar to the Mach 3 case, but there are some striking differences in this flowfield.

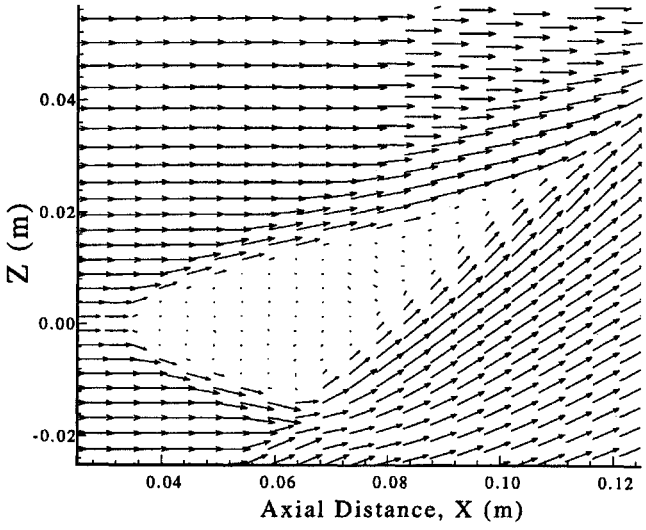

Fig. 12 Detailed view of velocity vectors in $Y = 0$ plane for run 3.

It is seen that the bubble shock lies much closer to the recirculation region and that the transmitted shock lies at a shallower angle. Both these observations can be attributed to the higher Mach number of this flowfield. In comparison to the Mach 3 case, the upper portion of the oblique shock is curved and, hence, results in a more pronounced upstream displacement.

A breakdown length, defined as the distance from the nose of the bubble shock to the point where the slip surface intersects the centerline, is used as an approximate measure of the severity of the strong interaction. It is assumed that a more severe interaction will lead to a larger breakdown length. For runs 9, 5, 3, and 12, which result in vortex breakdown, the breakdown length is 1.9, 1.8, 4.5, and 5.25 cm, respectively. A breakdown length for run 6 could not be obtained, as this interaction is so severe that the breakdown location extends up to the inflow boundary and contaminates the boundary conditions. Table 3 shows the values of λ and μ for each of these cases, and it can be seen that either of these parameters is a better indicator of the interaction than either S or τ. Runs 5 and 9 have comparable breakdown lengths, and as such, their values of λ and μ are also comparable.

Conclusions

Oblique shock/vortex interactions have been simulated using the three-dimensional, unsteady, compressible Euler equations, and the effects of Mach number, vortex strength, and streamwise velocity deficit on the interaction have been studied.

In the current work, the interaction between an oblique shock and a vortex whose axial velocity distribution is uniform ($\Phi = 1$) typically results in a weak interaction. In this type of interaction, the nonuniform region within the vortex leads to a distortion of the shock to form a convex-concave shape. Furthermore, the vortex tends to pass through the shock with minimal change in its strength and structure and is deflected at the same angle as the rest of the flow behind the shock. Among the weak interactions, it is found that if the distortion to the shock is great enough, expansion waves are generated near the interaction region and travel toward to the lower boundary.

In most of the cases studied in this work, decreasing Φ (or increasing the velocity deficit) typically results in a progressively stronger interaction. Initially, a moderate interaction is produced, in which the vortex distorts the shock to such an extent as to form a pocket of subsonic flow immediately behind the shock. It is speculated that this subsonic region, being generated by a strong oblique shock,

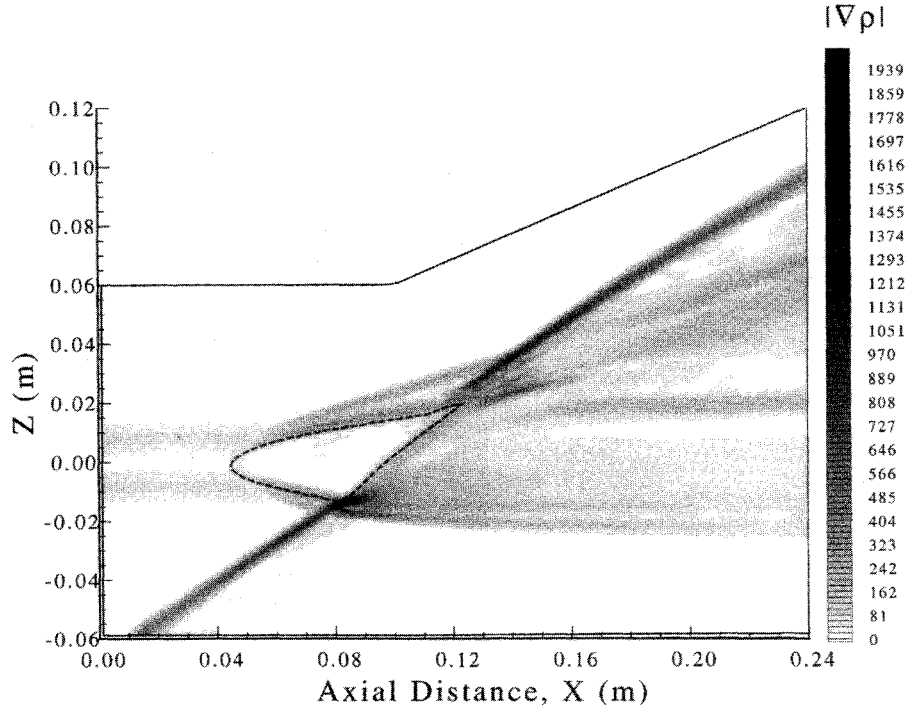

Fig. 13 Computational schlieren in $Y = 0$ plane for run 12 with a superimposed Mach 1 contour. Units of $\nabla\rho$ are 1/m.

does not allow any information to propagate upstream, and as a result, the incident vortex does not break down. However, there is an appreciable distortion of the vortex, which eventually splits into two counter-rotating vortices.

It appears as though the moderate interaction acts as a transition between the weak and strong interaction. As the axial velocity or Mach number deficit is increased, the local Mach numbers within the vortex, which are supersonic but much lower than the freestream Mach number, cannot be sustained by the high pressure gradient. As a result, the flowfield becomes locally subsonic near the interaction region and allows upstream information propagation. The subsonic region eventually consists of recirculating flow and a stagnation point at the axis of the vortex. The subsonic region behaves as a blunt obstruction to which the supersonic flow responds by creating a three-dimensional, separated shock structure. The characteristics associated with vortex breakdown, namely, the formation of a stagnation point on the vortex axis, followed by a region of flow reversal and the disruption of the incident vortex, are all observed in the strong interactions. The bubble shock interacts with the undisturbed oblique shock and creates a highly complicated, three-dimensional flowfield. In contrast to the weak and moderate interactions, where the flowfield is steady, the strong interactions result in an unsteady flowfield. It is believed that the recirculation region contributes to the apparent unsteadiness. Once the bubble shock reaches an equilibrium position, it is found that the location of the bubble shock oscillates at most by about 0.002 m, which is smaller than the vortex core radius. Without conducting a time-accurate simulation of this interaction, a determination cannot be made whether the unsteadiness is physical or is caused as an artifact of the numerical algorithm. Furthermore, since these calculations are simulated with the Euler equations, it is surmised that the unsteadiness might be caused because the Euler equations contain no natural dissipation.

This study has found that the velocity or Mach number deficit within the vortex plays a significant role in instigating vortex breakdown. Furthermore, it has been determined that traditional vortex strength parameters such the swirl parameter S or swirl ratio τ are not adequate to predict the strength of the interaction. Since the axial Mach number deficit has a profound effect on the interaction, it was found that S/Φ^3 or τ/Φ^3 is a better predictor of the interaction. For example, runs 1 and 3 are at the same Mach number and have the same value of Γ_0, but the former results in a weak interaction, whereas the latter results in a strong interaction. The difference between these two cases is the Mach number deficit, and one would expect that the vortex with an axial velocity deficit would result in a stronger interaction. This trend is predicted by noting that run 3 has a much higher value of λ than run 1. In the most general case, the OSVI depends on the vortex strength, the axial velocity deficit, freestream Mach number, and the shock strength, and a huge number of runs will need to be performed to arrive at an adequate vortex breakdown limit.

Acknowledgments

This work is funded by the NASA Center for Hypersonic Education and Research under Grant NAGw 3715, with Isaiah Blankson as Technical Monitor. The authors thank Donald P. Rizzetta, of the Wright Laboratory, for his invaluable assistance and especially for his identification of the vortex properties leading to breakdown. Gratitude is also expressed to Ashwani K. Gupta, of the Mechanical Engineering Department, and Josef Rom, of the Technion–Israel Institute of Technology, for their many helpful suggestions, and to James D. Baeder, Naruhisa Takashima, and Michael Frame for their technical assistance. Further appreciation is expressed to James E. Randolph and the Jet Propulsion Laboratory for the generous allocation of Cray Y-MP time.

References

[1]Zatoloka, V. V., Ivanyushkin, A. K., and Nikolayev, A. V., "Interference of Vortexes with Shocks in Airscoops. Dissipation of Vortexes," *Fluid Mechanics, Soviet Research*, Vol. 7, No. 4, 1978, pp. 153–158.

[2]Benjamin, T. B., "Theory of the Vortex Breakdown Phenomenon," *Journal of Fluid Mechanics*, Vol. 14, Dec. 1962, pp. 593–629.

[3]Hall, M. G., "Vortex Breakdown," *Review of Fluid Mechanics*, Vol. 4, 1972, pp. 195–218.

[4]Leibovich, S., "Vortex Stability and Breakdown: Survey and Extension," *AIAA Journal*, Vol. 22, No. 9, 1984, pp. 1192–1206.

[5]Delery, J. M., "Aspects of Vortex Breakdown," *Progress in Aerospace Sciences*, edited by A. D. Young, Vol. 30, Pergamon, Oxford, England, UK, 1994, pp. 1–59.

[6]Delery, J., Horowitz, E., Leuchter, O., and Solignac, J. L., "Fundamental Studies on Vortex Flows," *La Recherche Aérospatiale* (English edition), No. 2, 1984, pp. 1–24.

[7]Metwally, O., Settles, G., and Horstam, C., "An Experimental Study of Shock Wave/Vortex Interaction," AIAA Paper 89-0082, Jan. 1989.

[8]Cattafesta, L. N., and Settles, G., "Experiments on Shock/Vortex Interacton," AIAA Paper 92-0315, Jan. 1992.

[9]Kalkhoran, I. M., "Vortex Distortion During Vortex-Surface Interaction in a Mach 3 Stream," *AIAA Journal*, Vol. 32, No. 1, 1994, pp. 123–129.

[10]Kalkhoran, I. M., Smart, M. K., and Betti, A., "Interaction of Supersonic Wing Tip Vortices with a Normal Shock," AIAA Paper 95-2283, June 1995.

[11]Kalkoran, I. M., "Airfoil Pressure Measurements During Oblique Shock-Wave/Vortex Interaction in a Mach 3 Stream," *AIAA Journal*, Vol. 32, No. 4, 1994, pp. 783–788.

[12]Smart, M. K., and Kalkhoran, I. M., "The Effect of Shock Strengh on Oblique Shock Wave-Vortex Interaction," AIAA Paper 95-0098, Jan. 1995.

[13]Corpening, G., and Anderson, J. D., Jr., "Numerical Solutions to Three-Dimensional Shock Wave/Vortex Interaction at Hypersonic Speeds," AIAA Paper 89-0674, Jan. 1989.

[14]Rizzetta, D. P., "Numerical Simulation of Oblique Shock-Wave/Vortex Interaction," AIAA Paper 94-2304, June 1994.

[15]Rizzetta, D. P., "Numerical Investigation of Supersonic Wing-Tip Vortices," AIAA Paper 95-2282, June 1995.

[16]McGrory, W. D., Slack, D. C., Applebaum, M. P., and Walters, R. W., *GASP Version 2 User's Manual*, Aero Soft, Inc., Blacksburg, VA, 1992.

[17]Roe, P. L., "Approximate Riemann Solvers, Parameter Vectors, and Difference Schemes," *Journal of Computational Physics*, Vol. 43, No. 2, 1981, pp. 357–372.

[18]Roe, P. L., "Some Contributions to the Modelling of Discontinuous Flows," *Proceedings of the 1983 AMS-SIAM Summer Seminar on Large Scale Computing in Fluid Mechanics*, Vol. 22, Lectures in Applied Mathematics, Society for Industrial and Applied Mathematics, Philadelphia, PA, 1985, pp. 163–193.

[19]Hoffmann, K. A., and Chiang, S. T., *Computational Fluid Dynamics for Engineers*, Vol. 1, Engineering Education System™, Wichita, KS, 1993.

[20]Cattafesta, L. N., "An Experimental Investigation of Shock/Wave Vortex Interaction," Ph.D. Thesis, Dept. of Mechanical Engineering, Pennsylvania State Univ., University Park, PA, Dec. 1992.